# Influence of grain shape on the mechanical behaviour of granular materials

K. Szarf, G. Combe*, P. Villard

*Université de Grenoble - Laboratoire Sols, Solides, Structures - Risques (3S-R, UJF-INPG-CNRS UMR 5521) Domaine Universitaire BP53 38041 Grenoble Cedex 9 - France*

**Abstract**

We performed series of numerical vertical compression tests on assemblies of 2D granular material using a Discrete Element code and studied the results in regard to the grain shape. The samples consist of 5000 grains made either of 3 overlapping discs (clump - grain with concavities) or of six-edged polygons (convex grain). These two types of grains have a similar external envelope, ruled with a geometrical parameter $\alpha$. In the paper the applied numerical procedure is briefly described followed by the description of the granular model used. Observations and mechanical analysis of dense and loose granular assemblies under isotropic loading are made. The mechanical response of our numerical granular samples is studied in the framework of the classical vertical compression test with constant lateral stress (biaxial test). The macroscopic responses of dense and loose samples with various grain shapes comparison show that the shear resistance of a sample made of clumps increase with the grains concavity. Dense samples made of polygons are less dependant on the particle shape. This observation is not valid for loose samples made of polygons. The micromechanical origins of these results are explored by contact analysis, focusing especially on dense samples made of clumps: grain concavity furthers particles imbrications and increase shear resistance. Finally we present some remarks concerning the kinematics of the deformed samples. Whereas polygon samples submitted to a vertical compression present large damage zones (whatever polygons shape), dense samples made of clumps always exhibit thin reflecting shear zones caused by clump imbrications only, even if our granular model is cohesionless.
This work was done as a part of CEGEO research project[1]

*Key words:* DEM, grains shape, clumps of discs, polygons, isotropic compression, vertical compression, friction angle, shear localisation
*PACS:* 04.60.Nc, 81.05.Rm, 45.70.-n

## 1. Introduction

A typical numerical approach to discrete element modelling of granular materials is to use simple forms of particles (discs in 2D [1] or spheres in 3D [2]). Although the computation time is short that way, these models are not able to reflect some of the more complex aspects of real granular media behaviour, such as high shear resistance or high volumetric changes [3]. In order to model it properly either numerical parameters (intergranular rolling resistance [4, 5, 6]) or other grain shapes (aggregate of spheres [7] or polyhedral grains [8]) have to be used. The influence of grain shape is not fully understood yet. In this paper we wanted to present our investigations concerning the influence of grain shape on the mechanical behaviour of granular assemblies, grain concavity in particular. We compared two groups of grains - convex irregular polygons and non-convex clumps made of three overlapping discs.

[1] www.granulo-science.org/CEGEO

*Corresponding author
*Email address:* gael.combe@ujf-grenoble.fr (G. Combe)

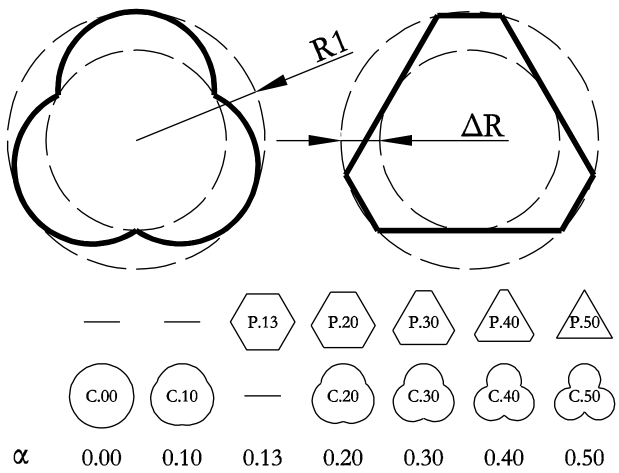


Figure 1: Particle shape definition: $\alpha = \Delta R/R_1$ and examples of particle shapes used for clumps and for polygons

## 2. Granular Model

The granular model used consists of 5000 polydisperse 2D frictional particles. Two kind of grain shapes are used: convex irregular polygons of six edges and non-convex particles made of aggregate of three overlapping discs named *clump*. These two shapes were chosen because of the similarity of their global contour (polygonal grains can be seen as a polygonal envelope of clumps made of three discs). As shown in figure 1, particles shapes are defined by a parameter $\alpha = \frac{\Delta R}{R_1}$ where $R_1$ denotes the particle excircle radius and $\Delta R$ is the difference between the ex- and the incircle radii. The incircle has to be contained in the particle fully. For non-convex clumps $\alpha$ ranges from 0 (circle) to 0.5. For convex polygonal grains $\alpha$ ranges from $1 - \frac{\sqrt{3}}{2} \simeq 0.13$ (regular hexagons) to 0.5 (equilateral triangles). Some of the shapes used are presented in the table in Fig. 1. For each chosen $\alpha$, granular samples are made of polydisperse particles. The polydispersity of grains is driven by the radii of the grain excircle. In each sample, the chosen radii $R_1$ are such that the areas of the excircle are uniformly distributed between $S_m = \pi R_m^2$ and $S_M = \pi(R_M)^2 = \pi(3R_m)^2$.

## 3. Discrete Element Method

Two-dimensional numerical simulations were carried out using a discrete element method [9] within the framework of *Molecular Dynamics* (MD) principles [10]. Grains interact in their contact points with a linear elastic law and a Coulomb friction. The normal contact force $f_n$ is related to the normal interpenetration (or overlap) $h$ of the contact as

$$f_n = k_n \cdot h \quad , \tag{1}$$

$f_n$ vanishes if contact disappears, i.e. $h = 0$. The tangential component $f_t$ of the contact force is proportional to the tangential elastic relative displacement, with a stiffness coefficient $k_t$. The Coulomb condition $|f_t| \leq \mu f_n$ requires an incremental evaluation of $f_t$ in every time step, which leads to some amount of slip each time one of the equalities $f_t = \pm\mu f_n$ is imposed ($\mu$ correspond to the contact friction coefficient). A normal viscous component opposing the relative normal motion of any pair of grains in contact is also added to the elastic force $f_n$. Such term is often introduced to ease the approach of mechanical equilibrium. In case of frictional assemblies under quasistatic loading, the influence of this viscous force (which is proportional to the normal relative velocity using a damping coefficient $g_n$) is not significant [11] (elastic energy is mainly dissipated by Coulomb friction). Finally, the motion of grains is calculated by solving Newton's equations using a third-order predictor-corrector discretisation scheme [12].

Principles of discs contact detection are well known [13], and contact detection for clumps was solved as for discs: a contact occurs in a point, the normal force value $f_n$ is computed with eq. (1) and its direction

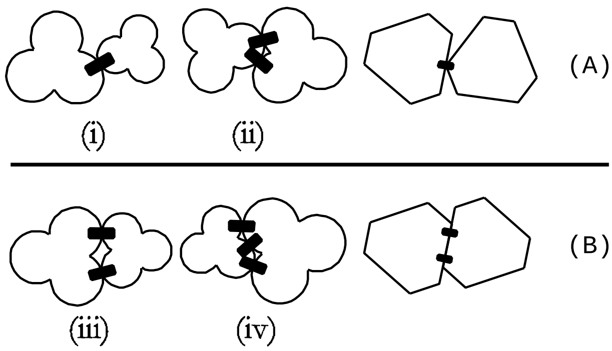


Figure 2: Contact types for clumps and polygons: *corner-to-edge* (A) and *edge-to-edge* (B). This figure also show that for a contact between two polygon edges, two contact points are considered. Only one is considered if there is a contact between an edge and a corner

connects the centres of discs in contact, Fig. 2. Contact detection and contact forces calculations between polygons do not use classical methods based on the area overlap between polygons [14, 15, 16, 17]. Instead they use the *shadow overlap* technique proposed by J.-J. Moreau [18] which was originally applied within the *Contact Dynamic* approach [19] for convex polygonal particles. In our study, this technique is adapted to the MD approach. Three geometrical contacts can exist between polygons: corner-to-corner, edge-to-corner and edge-to-edge contact. Corner-to-corner contacts are geometrically (or mathematically) realistic but never occur in our simulations because of numerical round errors. When dealing with edge-to-edge contact, *shadow overlap* involves two contact points and their associated overlap $h$, figure 2. This is the main difference with the classical method (area overlap calculations) where only one contact is considered between edges.

Finally, one may be interested in the main contact law parameters: the normal and tangential stiffness: $k_n$ and $k_t$, and the friction coefficient $\mu$. Assuming that samples would be loaded with a 2D isotropic stress $\sigma_0 = 10$ kN/m, the normal stiffness of contact $k_n$ was computed according to the dimensionless 2D *stiffness parameter* $\kappa = k_n/\sigma_0$ [20, 11, 21], which express the mean level of contact deformation ($1/\kappa$). $\kappa$ was arbitrarily set to 1000. As a comparison, a sample made of glass beams under an isotropic loading of 100 kPa reach $\kappa = 3000$. The tangential stiffness $k_t$ can be expressed as a fraction of the normal stiffness, $\tilde{k} = k_t/k_n$, $\tilde{k} > 0$. In discrete element literature $\tilde{k}$ is often equal one. $\tilde{k} > 1$ can presents specific behaviour where *Poisson coefficient* of grain assemblies become negative, [22, 23, 24, 25]. Running several numerical simulations with various $\tilde{k}$, $0 < \tilde{k} \leq 1$, [20] have shown that if $0.5 \leq \tilde{k} \leq 1$, the macroscopic behaviour remains similar. Thus we arbitrarily fixed $\tilde{k}$ to 1.

## 4. Sample Preparation - Isotropic Compression

Granular samples of 5000 grains are prepared in three steps: preparations start with a random spatial distribution of the particles inside a square made of four rigid walls. Next the particles slowly grows until $\sigma_0 = 0.5$ kN/m is reached. Finally, samples are isotropically loaded by wall movement up to $\sigma_0 = 10$ kN/m. Fragments of two samples[1] *C.30* and *P.30* (clumps and polygons with $\alpha = 0.3$) are displayed in figure 3.

In presence of rigid boundary conditions like walls this second step of the preparation is the only way to ensure a good homogeneity of the contacts-forces network and the contact density. This was successfully checked in every sample and furthermore we systematically observed that contact orientations (fabric tensor) were isotropically distributed in every directions of the plane. To obtain samples with different compacities one may use various values of the intergranular friction coefficient $\mu$, [26]. During the preparation phase with $\mu$ fixed to zero, samples isotropically loaded up to $\sigma_0 = 10$ kN/m are dense and the compacity is

[1]Samples will be denoted *C.xx* or *P.xx* respectively for *C*lumps and *P*olygons, where *.xx* correspond to the decimal part of the shape number $\alpha$

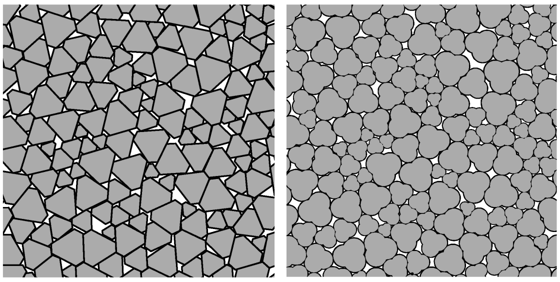

Figure 3: Fragments of two samples submitted to an isotropic loading $\sigma_0 = 10$ kN/m. Sample *P.30* on the left and *C.30* on the right. shape parameter $\alpha = 0.3$

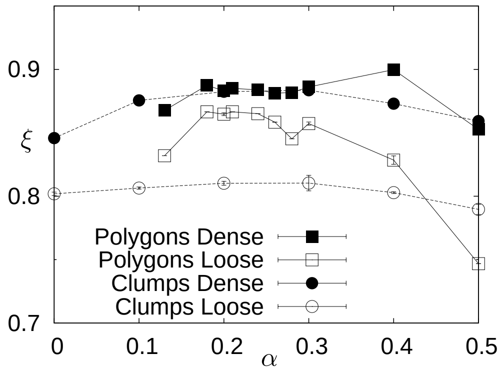


Figure 4: Compacity $\xi$ versus $\alpha$ of samples under isotropic loading. Error bars correspond to standard deviation computed over a population of four samples. Round and square symbols represent samples made of clumps and of polygons respectively. Black and white symbols represent dense and loose sample respectively

*maximal*. When instead a positive value of $\mu$ is used, samples became looser and compacity decrease. In our study dense samples were prepared with $\mu = 0$ and the loose ones with $\mu$ equal 0.5. 16 different samples (4 denses, 4 looses made of clumps and 4 denses, 4 looses made of polygons) for each $\alpha$ value were prepared[2]. Figure 4 show that samples made of polygons *P.xx* are as dense as *C.xx* samples when the friction coefficient used during the isotropic compression is null. When samples are looser, $\mu = 0.5$, *P.xx* samples show bigger compacity than *C.xx* samples: intergranular friction seems to prevent clumps imbrication and thus generate more voids in samples than polygons for which grains envelope is convex.

For both clumps and polygons, contact between particles can occur in more that one contact point. For clumps there are four contact possibilities: single contact Fig.2(i), double contact involving three discs Fig.2(ii), triple contact Fig.2(iii) and a double contact involving four discs Fig.2(iv). By analogy with polygon contacts (edge-to-edge or corner-to-edge, Fig.2) all these contacts between clumps can be merged in two groups, (A) and (B). Other groups may also be defined, for example *simple* contacts which correspond to single contacts (Fig.2(i)) for clumps and polygons - group (A'); *complex* contacts which correspond to contact (ii)+(iii)+(iv) for clumps and double contact for polygons - group (B'). One can imagine that $\alpha$ can have a large influence on the proportion of contact types.

We studied the *coordination number* $z^*$ corresponding to the mean number of contacts per grain. Here only grains that support two or more compression forces, and therefore take part in load transfer, were considered. For samples made of frictionless perfectly rigid discs, $z^*$ is equal exactly 4 [27]. Because $\kappa$ is not

[2]All analysis will be done on mean results computed over 4 samples of each shape and each $\alpha$. Associated Standard Deviations will always be given, even if they are to small to be significant.

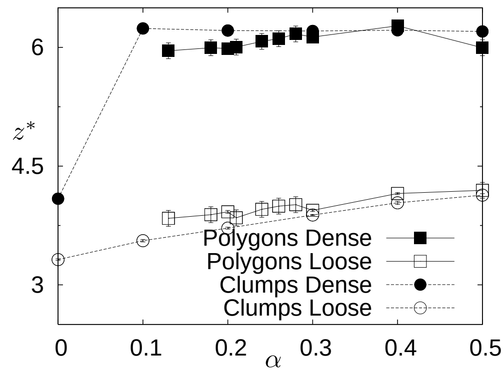


(A')

Figure 5: Coordination number $z^*$ values vs. $\alpha$ under an isotropic loading. Round and square symbols represent samples made of clumps and of polygons respectively. Black and white symbols represent dense and loose sample respectively

infinite in our study, $z^* = 4.093 \pm 0.005$ is greater in our samples made of circular particles (discs, $\alpha = 0$), but still very close to the reference value. $z^*$ is evaluated for clumps and polygons, both dense and loose samples. The dependence of $z^*$ along $\alpha$ is shown in figure 5. It is typical to observe high value of $z^*$ for samples prepared without friction, as the ones presented. Dense samples made of frictionless clumps show constant values of $z^*$ for all the shapes. Dense samples made of polygons show similar tendency. This can be probably explained by the grain envelope similarity of the two groups and because we used a double contact technique at every polygon edge-to-edge contact. What is more, $z^*$ increase linearly with $\alpha$ when samples are prepared with positive friction coefficient $\mu = 0.5$.

## 5. Macro-mechanical Response of Granular Assembly Loaded in Vertical Compression Test

The samples were tested in a 2D strain controlled vertical compression test. The vertical stress $\sigma_1$ was increasing while lateral $\sigma_3$ remained constant. The loading velocities were chosen according to the *inertial number* $I = \dot{\varepsilon}_1\sqrt{\frac{\langle m \rangle}{\sigma_3}}$ [21] where $\dot{\varepsilon}_1$ denotes the strain rate and $\langle m \rangle$ is the typical mass of a grain. $I$ value was set to $5 \cdot 10^{-5}$. It describe the level of dynamic effects in the sample. For quasi-static states value of $I$ should be low. The mechanical responses of the samples are plotted on $\eta$ vs. $\varepsilon_1$ charts and shown in figure 6. $\eta = t/s$, $t = (\sigma_1 - \sigma_3)/2$ is the half of the deviator stress and $s = (\sigma_1 + \sigma_3)/2$ is the mean stress.

For dense samples *C.xx* made of clumps, one can observe in figure 6(a) that the macroscopic shear resistance increase with $\alpha$. The $\eta$-$\varepsilon_1$ curve for discs is also shown in figure 6(a). Although *C.10* implies grains with a small $\alpha$, the mechanical response of that sample exhibit remarkable increase of the maximum deviator in comparison to discs samples *C.00*. Extracted from $\eta$-$\varepsilon_1$ curves, friction angles at the peak $\phi_p$ and at the threshold $\phi_t$ are shown in the figure 7(a). For loose clump samples there is no peak value of the friction angle, $\phi_p = \phi_t$, figure 6(c). Thus, for all *C.xx* samples, the trend is: both peak $\phi_p$ and threshold $\phi_t$ friction angle values increase along with $\alpha$. $\phi_t$ increase proportionally while $\phi_p$ of dense samples increase is nonlinear and seems to be asymptotic for larger $\alpha \geq 0.4$.

For dense *P.xx* samples, the analysis of $\eta$-$\varepsilon_1$ curves presented in Fig. 6(b), show that $\phi_p$ values slightly decrease linearly along with $\alpha$, while $\phi_t$ values increases, Fig. 7(a). For loose *P.xx*, depending on $\alpha$, one can notice macroscopic curves characteristic to loose samples but dense as well , Fig. 6(d). Then, the tendency is more complex: when $\alpha \leq 0.3$, every sample present different values of $\phi_p$ and $\phi_t$. On the contrary, there is no peak when $\alpha > 0.3$ and $\phi_p = \phi_t$. This kind of the behaviour can be correlated probably to the initial compacity of the samples shown in figure 4 and where one can observe that $\xi$ values are close for dense and loose *P.xx* samples when $\alpha \leq 0.3$. If we focus only on $\phi_t$ for loose *P.xx*, we observe an increase of the friction

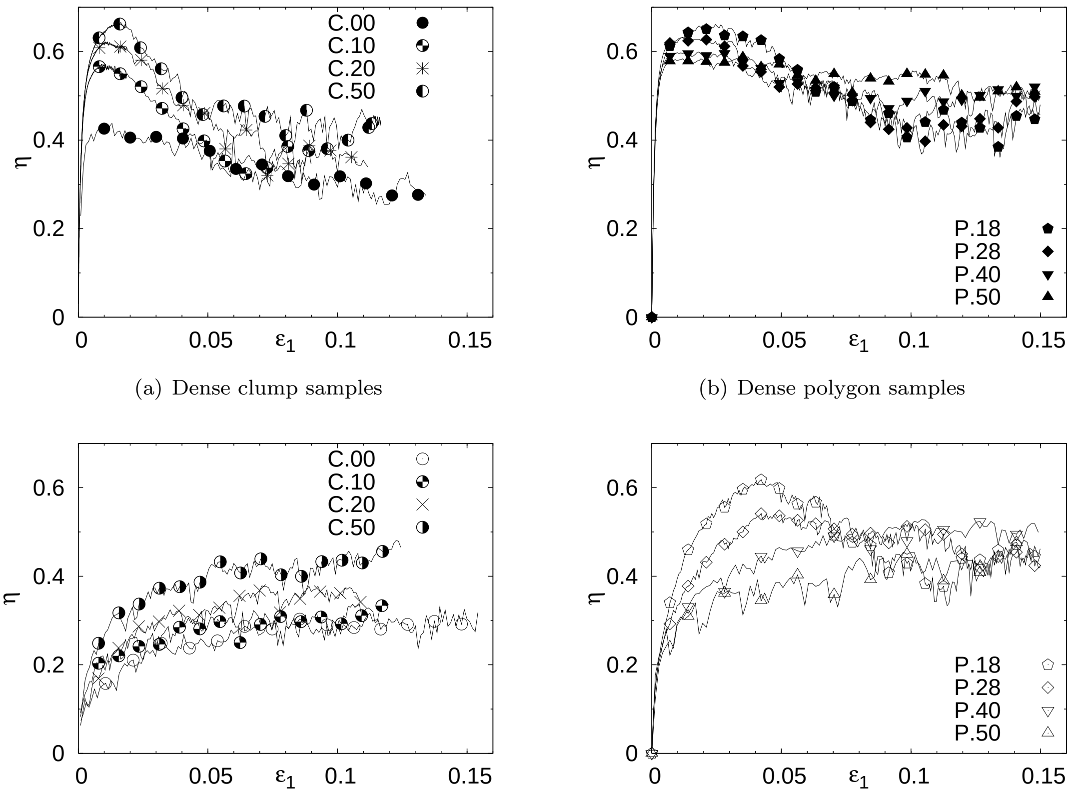


(a) Dense clump samples

(b) Dense polygon samples

(c) Loose clump samples

(d) Loose polygons samples

Figure 6: Macroscopic $\eta - \varepsilon_1$ curves for some of the samples

angle with $\alpha$, except for samples made of triangles, $\alpha = 0.5$, which always behave specifically[3].

To sum up the observations made on threshold friction angles for clumps and polygons with constant $\mu$, adding some particles irregularity by increasing $\alpha$ always lead to an increase of the macroscopic angle of friction in the critical state. This influence of the grain geometry is in agreement with a previous study of Salot et al. [7]. Lastly, as one can see in figure 6, there isn't any obvious influence of $\alpha$ on the Young's modulus. $E$ is linked to the rigidity matrix and therefore to $z^*$ [28], which is constant for dense samples (Fig.5).

In figure 8, volumetric changes of some samples are shown. For both dense clump and polygons samples, Fig. 8(a) and 8(b), the volume[4] increase mainly during the vertical compression, after a small contraction due to the stiffness of the contacts [11]. The volumic increase for dense $C.xx$ samples is quite similar from one chosen $\alpha$ to another. On the other hand, $\alpha$ clearly influence the volumetric change of dense $P.xx$ samples but this influence seems erratic. Nevertheless, dense $P.xx$ samples show bigger total dilatancy than dense $C.xx$ samples. Loose $C.xx$ sample behave like loose sands and are contractant during the whole compression tests. It is more complex for loose polygon samples: as said previously about $\eta$-$\varepsilon_1$ curves, loose $P.xx$ samples behave like loose granular materials when $\alpha \geq 0.4$, and as a consequence, samples are then contractant. When $\alpha < 0.4$, samples always increase their volume.

There is no particular influence of particle concavity on average dilatancy angle $\psi$ values ($\sin\psi = \frac{d\varepsilon_1 + d\varepsilon_3}{d\varepsilon_1 - d\varepsilon_3}$)

[3]Notice that triangle is the only shape with 3 edges.

[4]Which is in fact an area in 2D but here called volume.

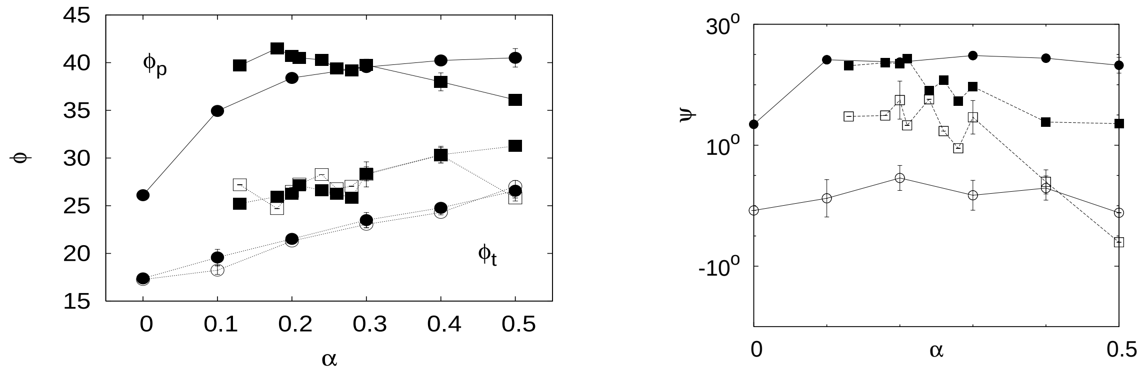


(a) Friction angles

(b) Dilatancy angles

Figure 7: (a) - Friction angles vs $\alpha$ for clumps and polygons samples. The two upper curves correspond to friction angle at the peak $\phi_p$ of dense samples. The four other curves show friction angles at the threshold $\phi_t$, either for dense and loose samples. (b) - Dilatancy angles for all the samples; Values of the angles for dense samples were computed at the peak, between [1,5 - 2,5%]$\varepsilon_1$; For loose ones the range was [6-7%]$\varepsilon_1$. On both figures, circular and square symbols refer respectively to samples made of clumps and polygons. Black symbols indicate dense samples and loose samples with white ones

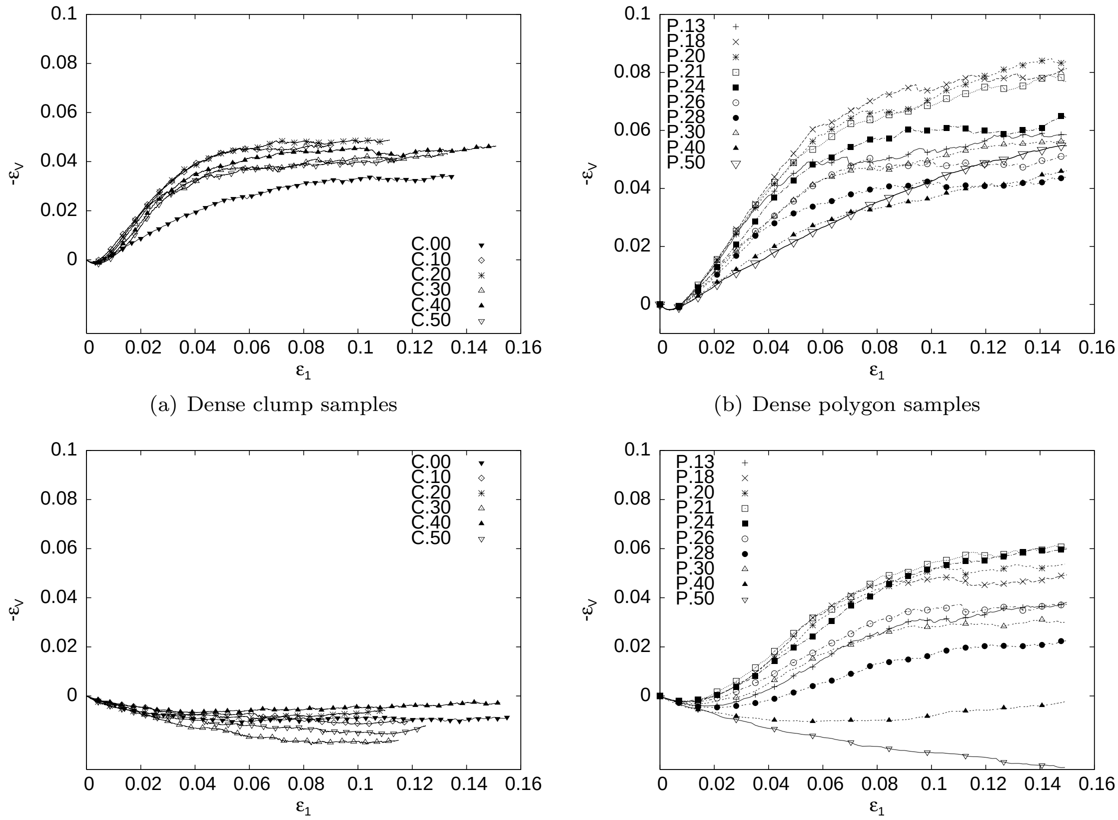


(a) Dense clump samples

(b) Dense polygon samples

(c) Loose clump samples

(d) Loose polygons samples

Figure 8: Volumetric changes (computed in 2D it correspond to the area) during vertical compression for loose and dense samples made of clumps and of polygons. Positive $-\varepsilon_v$ implies an increase of the sample volume

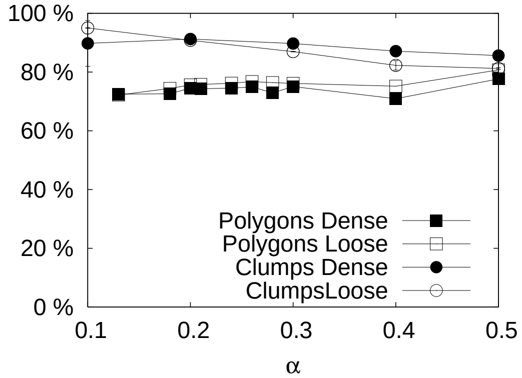


Figure 9: Corner-to-edge contacts (*(B)* contact, see Fig. 2) percentage at the end of the vertical compressions. Comparison between clumps and polygons

of clump samples, both dense and loose (Fig.7(b)). On the other hand, $\psi$ is lower for polygons with higher values of $\alpha$ than for the ones more similar to hexagons.

## 6. Micromechanical Analysis

### *6.1. Contact Proportion Evolution*

A way to investigate and to try to explain the grain shape influence on the mechanical behaviour discussed in the previous section, is to focus on the particle scale. In order to do that, one can investigate the intergranular contact proportions at three stages of biaxial test: in the isotropic state, at the peak and in the critical phase.

Focusing on the critical phase firstly (end of the biaxial test), contacts observations based on the division to two contact groups edge-to-edge *(A)* and corner-to-edge *(B)* (Fig.2) can be made. The evolution of *(B)* contacts in function of $\alpha$ is shown in figure 9. *(A)* can be easily deduced by subtracting *(B)* percentage from 100. On one hand, the percentage of *(B)* contacts does not depend on the initial compacity of the sample, dense and loose samples present similar trend. One the other, *(B)* percentage for *C.xx* samples decrease linearly with $\alpha$. Opposite tendency is observed for *P.xx* samples. For $\alpha = 0.5$ clump and polygon shapes converge and this is probably the reason why *(B)* percentages are close.

Generally speaking the majority of contacts is single and it increase along $\varepsilon_1$. That is why the percentage of *(B)* contacts is higher than *(A)*. Because dense samples were prepared with no friction, compacity of each assembly of grains submitted to an isotropic loading is always maximum. As a consequence, even if samples are able to exhibit small contractancy (related to dimensionless contact stiffness $\kappa$), total number of contacts in each sample during a vertical compression systematically decrease. Therefore in order to be able to compare different contact type proportions we propose to balance the decrease in total contact number using a coefficient $\omega^* = N^*_{\varepsilon_b}/N^*_{\varepsilon_a}$, where $N^*_{\varepsilon_a}$ and $N^*_{\varepsilon_b}$ represent the total number of all neighbouring contacts[5] at a given stages ($\varepsilon_a$ or $\varepsilon_b$) in the sample. We propose here to focus on the evolution of two contact groups for clumps, previously defined in section 4:

- *(A')* single contact between grains, called *simple* contact,
- *(B')* multiple contacts between grains, called hereafter *complex* contacts.

[5] When two grains are in contact via 1, 2 or 3 contacts points, only one contact is counted.

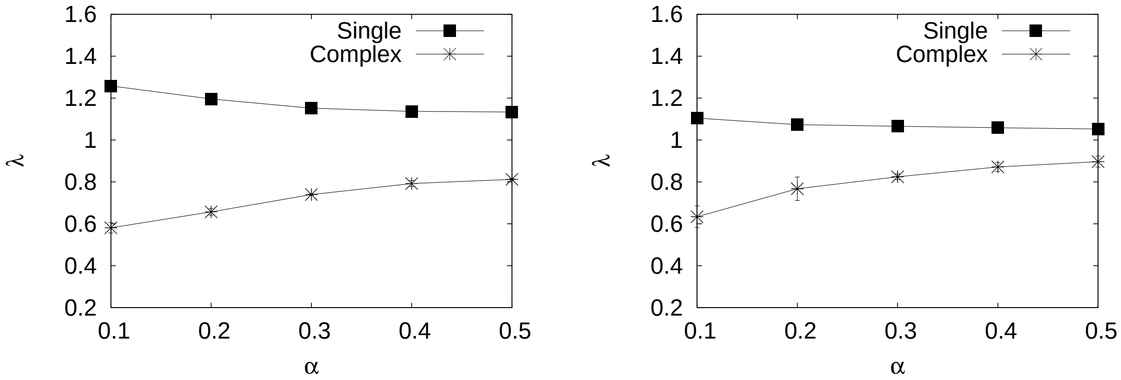


(a) (b)

Figure 10: Transformation of complex clump contacts to simple, quantified by $\lambda$ and evaluated between the maximum stress deviator (peak) and the isotropic initial state for figure (a), and between the peak and the critical state, Fig. (b)

We observed the evolution of clump contact number of each group between two successive stages and normalised that evolution with $\omega^*$. Thus we define a new variable $\lambda = \omega^* \cdot N^{\varepsilon_a}/N^{\varepsilon_b}$, where $N^{\varepsilon_a}$ and $N^{\varepsilon_b}$ denotes the number of *(A')* or *(B')* contacts between two different stages $\varepsilon_a$ and $\varepsilon_b$ of the vertical compression. In figure 10(a), we can observe that for $\alpha = 0.1$, $\lambda$ is smaller than 1 for complex *(B')* contacts and greater than 1 for simple *(A')*. These were computed between $\varepsilon_a$: isotropic state and $\varepsilon_b$: maximum stress deviator (peak). This can be analysed as a transformation of complex contacts into simple between these two stages. When all complex contacts transform into simple, graphical points are in equal distance from 1, $1 - \lambda_{(B')} = \lambda_{(A')} - 1$. If $1 - \lambda_{(B')} > \lambda_{(A')} - 1$, it means that some complex contacts transform in simple but some disappear as well. When $\alpha$ goes to 0.5 these transformations are still active but with less intensity. Geometrical imbrications between clumps increase with $\alpha$ and are "more difficult to lose" during biaxial test. $\lambda$ seems to reach a threshold when $\alpha \geq 0.4$, Fig. 10(a). This last observation may be correlated to the evolution of $\phi_p$ which also reach a threshold for the same value of $\alpha$, Fig. 7(a).

Focusing on $\lambda$ between the peak and the critical state, Fig. 10(b), we can observe that the increase of simple contacts is small for every $\alpha$ ($\lambda_{(A')} - 1 \simeq 0$) and complex contact are mainly lost $1 - \lambda_{(B')} > 0$, especially when $\alpha$ is small. Greater is $\alpha$, smaller is the amount of lost complex contacts (grains imbrication are destroyed less). This may explain that $\phi_t$ of clumps increase with $\alpha$, Fig. 7(a).

### *6.2. Contact Orientation Evolution*

Contact orientations and their evolutions during the vertical compression tests are classically analysed. Usually one can observe that contacts are lost in the extension direction and gained in the direction of compression, [29]. In figure 11 we present statistical analysis of contact orientations between different stages for two values of $\alpha$, by evaluation of $P(\theta) = N_{\varepsilon_b}(\theta)/N_{\varepsilon_a}(\theta)$, where $\varepsilon_a$ and $\varepsilon_b$ correspond to two successive stages, $N_{\varepsilon_x}(\theta)$ is the number of contacts in the direction $\theta$ for the stage $\varepsilon_x$; $P(\theta_i) = 1$ express that the number of contact in the direction $\theta_i$ remain constant between the two studied stages; if $P(\theta_i) < 1$, contacts are lost and if $P(\theta_i) > 1$ contacts are gained in $\theta_i$ direction. When we focus on the evolution of contact numbers between the isotropic state and the peak, Fig. 11(a) for $\alpha = 0.2$ and Fig. 11(c) for $\alpha = 0.5$, we can observe that there is no contact gain in any direction. $P(\theta) \simeq 1$ in the compression direction and $P(\theta) < 1$ indicate that most of the contacts are lost in the extension direction. Computed of $\theta$, the mean of $P$ is smaller than 1 for both $\alpha$ and we have checked that it is almost constant for all studies $\alpha$. This simply indicate that contacts are mainly lost during the vertical compression of dense samples made of clumps. Finally, we noticed that greater $\alpha$ is, bigger is the imbrication between grains and smaller is the amount of contacts lost in the extension direction.

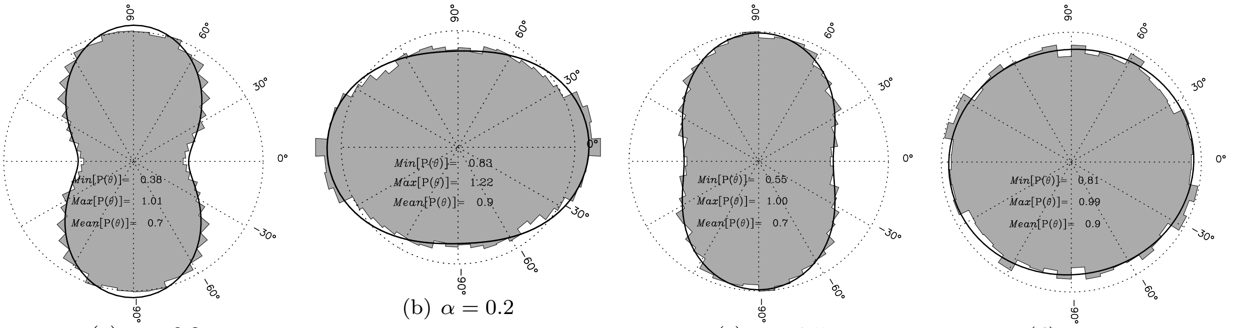


(a) $\alpha = 0.2$ (b) $\alpha = 0.2$ (c) $\alpha = 0.5$ (d) $\alpha = 0.5$

Figure 11: $P(\theta)$ computed between different stages, over 25 classes of 7.2°. Statistics computed over approximatively 40000 contacts for the isotropic state, 30000 contacts at the peak and 29000 at the critical state. The circle radius drawn in dash line is 1. (a) and (c): Isotropic state to the peak. (b) and (d): Peak to the critical state

Analysing contacts reorientation between the peak and the critical state, Fig. 11(b) and 11(d), exhibit opposite tendency because contacts are mostly lost in the compression direction and gained in the extension direction when $\alpha$ is small, Fig. 11(b). When $\alpha$ is bigger, contacts are lost in every direction, Fig. 11(d).

We proposed now the same contact orientation analysis but for *(A)′* and *(B′)* contact groups (simple and complex contacts). Statistical analysis of the evolution of contact orientation from the isotropic state to the peak for *(A)′* and *(B)′* groups is shown in figure 12. On one hand, Fig. 12(a) and 12(b) show that *(A')* contacts are gained ($\alpha = 0.2$) or are kept ($\alpha = 0.5$) in the compression direction; Simple contacts are mainly lost in the extention direction, especially when $\alpha$ is small. On the other hand, we can observe that *(B')* are lost in every directions with some variations depending on $\theta$. Nevertheless, complex contact are more persistent when $\alpha$ is greater (the mean of $P$ is bigger for $\alpha = 0.5$ because of grain imbrications).

The statistical analysis of the evolution of contact orientations between the peak and the critical state, Fig 13, confirm the tendency seen in figures 11(b) and 11(d): when $\alpha$ is small, simple and complex contacts are lost in the compression direction, especially for *(B')* contact group. One can also notice that the mean of $P$ is equal to 1 for figure Fig 13(a), $\alpha = 0.2$, and lower than 1 in figure 13(c), the number of simple contacts remains constant during the mechanical test from the peak to the critical state. When $\alpha = 0.5$, the number of simple contacts decreases, the mean of $P$ is 0.9. *(B')* contacts are those which are mainly lost. All these observations can be correlated to figure 10, where the different roles of simple and complex contacts were already pointed out.

Loosing and gaining contacts respectively in the compression and the extension direction is not a classical result, even between the peak and the critical state, [29]. This should be analysed as a pathology of dense samples prepared without intergranular friction.

### *6.3. Shape Influence on Local Strain Analysis*

We focused on the strain localisation in the samples in order to study the macroscopic rupture and its origins. Two approaches were used for that: *local strain maps* and *shear localisation indicator* $S_2$ [30]. Comparing particle kinematics in the isotropic state $\varepsilon_a$ and in a deformed stage $\varepsilon_b$ we computed local strains over Delauney triangulation like in [29]. Using the second strain invariant we illustrate the shear localisation in figure 14. The shear maps show that polygon samples create wide shearbands that develop slowly during the test. Clump behaviour is different, the localisation zones are more narrow and appear rapidly. This complies with the previous remarks about the overall dilatancy of the samples, see section 5 and Fig. 8.

Shear localisation indicator is defined as

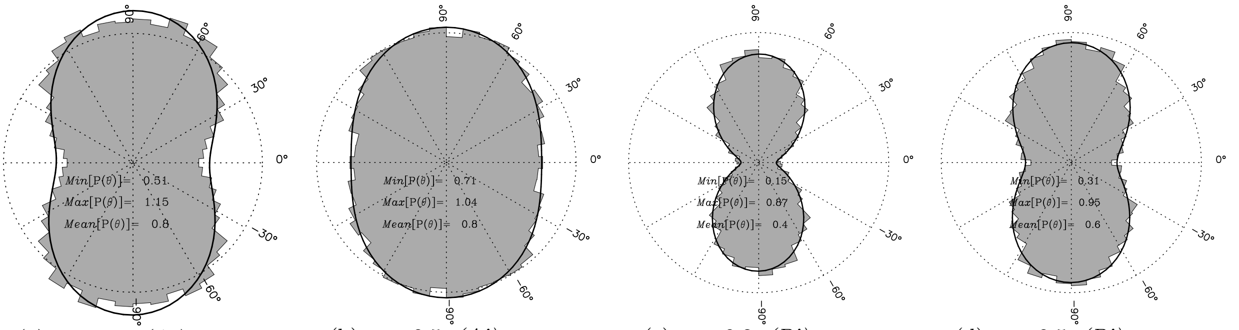


(a) $\alpha = 0.2$, *(A')* contacts (b) $\alpha = 0.5$, *(A')* contacts (c) $\alpha = 0.2$, *(B')* contacts (d) $\alpha = 0.5$, *(B')* contacts

Figure 12: $P(\theta)$ computed between the isotropic state and the peak, over 25 classes of 7.2°. The circle radius drawn in dash line is 1

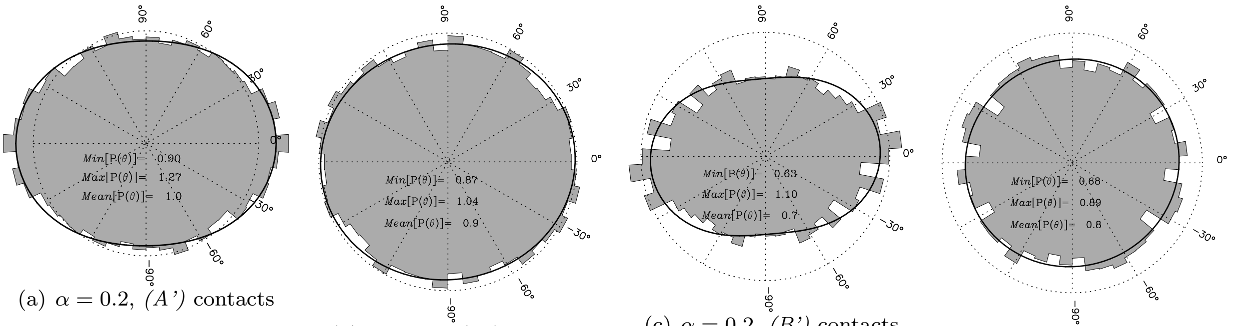


(a) $\alpha = 0.2$, *(A')* contacts (b) $\alpha = 0.5$, *(A')* contacts (c) $\alpha = 0.2$, *(B')* contacts (d) $\alpha = 0.5$, *(B')* contacts

Figure 13: $P(\theta)$ computed between the peak and the critical state, over 25 classes of 7.2°. The circle radius drawn in dash line is 1

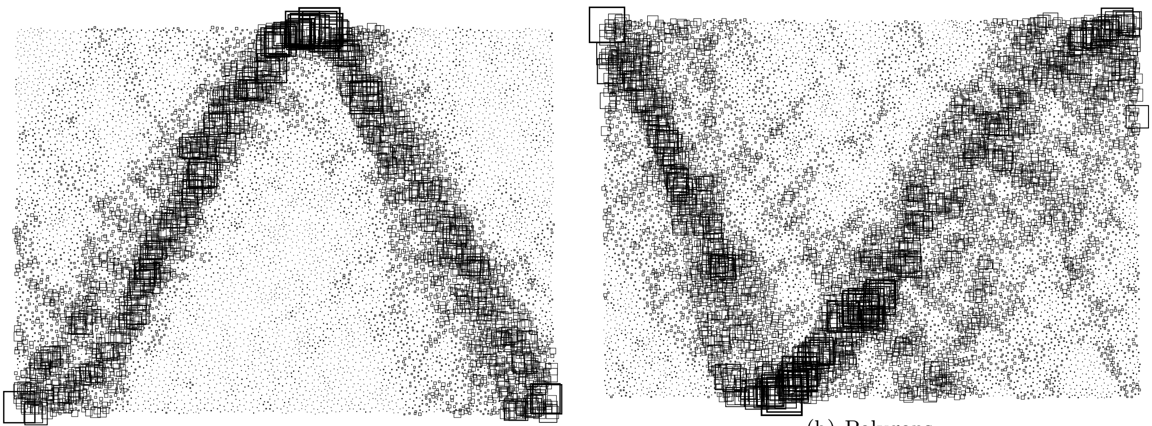

(a) Clumps (b) Polygons

Figure 14: Shearmaps on samples made of grains with $\alpha = 0.3$. $\varepsilon_1 = 0 \ - \ 13.5\%$

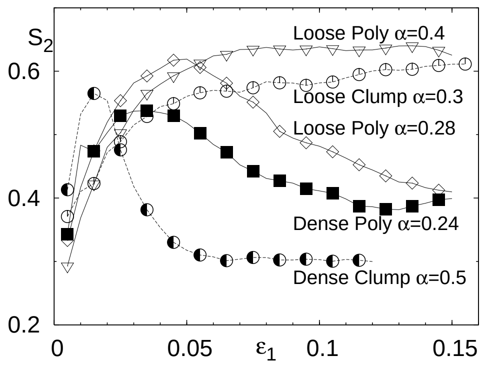


Figure 15: Shear indicator evolution during a vertical compression

$$S_2 = \frac{1}{N_t} \frac{\left( \sum_{i=1}^{N_t} I_{2\varepsilon} \right)^2}{\sum_{i=1}^{N_t} I_{2\varepsilon}^2} \tag{2}$$

where $I_{2\varepsilon}$ is the second invariant of the strain tensor and $N_t$ is the total number of triangles. In a sense, value of $S_2$ can be regarded as a percentage of a distorted sample area.

Figure 15 give the evolution of $S_2$ for several dense and loose samples made of clumps and polygons. Close to the isotropic state both groups behave similarly and the maximum value of $S_2$ is reached at about 2% of $\varepsilon_1$. At this stage at least half of the sample is distorted, $0.5 < S_2 < 0.6$. Later $S_2$ decrease, which indicates that $I_{2\varepsilon}$ localise in a focused zone. In figure 15, on can observe that the dense clumps sample with $\alpha = 0.5$ present a large decrease of $S_2$ and quickly reach a threshold value $S_2 = 0.3$ corresponding to a sheared area of 30%. On contrary, the evolutions of $S_2$ for the dense polygons sample with $\alpha = 0.24$ and the loose polygons sample with $\alpha = 0.28$ indicate that the localisations of sheared zones is more progressive along $\varepsilon_1$. For $\varepsilon_1 = 0.15$, these samples produced shear bands on 40% of their area. For the two loose samples for which $S_2$ evolutions are shown on figure 15, *C.30* and *P.40* samples, we observe an expanding sheared area up to $\varepsilon_1 = 0.8$. In these cases, we have check on shear maps that sheared zones, which correspond to more than 60% of the total area of the samples, are spread.

Analysing all our numerical simulations, in dense samples sheared zones are thinner for *C.xx* than for *P.xx* and appear earlier during a test. Dense samples made of polygons kinematically behave mostly like dense sands and clump samples like brittle material. The threshold values of $S_2$ are $10 - 20$% higher for dense polygon samples than for dense clumps of the same $\alpha$. What is more, the shape of $S_2$ curves is closely correlated with the shape of stress-strain curves. Positions and widths of the peaks overlap.

## 7. Conclusions

The aim of that article was to present our work in progress about the mechanical influences of particles shapes in granular assemblies in the framework of numerical simulations perfomed by Discrete Element Method. First, a grain geometry parameter $\alpha$ was defined. For particles called clumps and made of 3 overlapping discs, $\alpha$ is a measure of the grain concavity. 6-edged convex polygonal grains were also ruled by $\alpha$. The overall envelope depending on $\alpha$ for each type of particles used in the studied granular model was the common feature. Our numerical simulations were perfomed by discrete element method adapted to each type of grain shapes. For particles made of discs (clumps), the commercial code PFC$^{2D}$ of ITASCA by was used. For polygonal particles, we developed our own computer code which implement some special contact detection between objects in the framework of Molecular Dynamic approach. In this paper we highlighted that changing grain geometry influence granular assembly mechanical behaviour under the classical vertical compression test, also called *biaxial test* in 2D. More complex grain shapes allow reaching higher levels of internal friction angle and large volumetric strains comparing to discs. Some clear differences in the behaviour of polygons (convex) and clump (non-convex) assemblies were shown. One should notice also that the chosen shapes of particles demonstrate similarities as well, caused by the global envelope, that justify the comparison. Granular assemblies generation and compaction was presented. By the use of two extremes values of the intergranular friction angle $\mu$, dense and loose samples were prepared, both for samples made of clumps and polygons.

First, focusing on the macroscopic mechanical behaviour of our granular model we show that loose samples composed of polygons with low values of $\alpha$ present behaviour typical to consolided soils where the initial contractance stage was not only due to contact stiffness but also to large intergranular reorganisations. Apart from that, loose and dense samples of all shapes behave as expected (loose samples only show contractant behaviour while dense ones mostly exhibit large dilatancy), showing similar behaviour when discussing friction residual angle $\phi_t$ or percentage of contacts. All samples show higher values of maximum internal friction angle $\phi_p$ and $\phi_t$ than samples only made of circular grains (each particle is a disc). The correlations between shape parameter $\alpha$ and friction angles are different for clumps and polygons. On one hand, for dense clump samples, $\phi_p$ increase with $\alpha$ and seems to reach a assymptotic value $\phi_p = 40°$. On the other hand, $\phi_p$ linearly decrease when $\alpha$ goes from 0.13 to 0.5. On that occasion, the particular case of triangular shape ($\alpha = 0.5$) is also discussed briefly. Overall dilatancy of clump samples is bigger than the one of disc assemblies, but spectacularly smaller than dilatancy of polygons.

Secondly, at the granular scale, we proposed to correlate macroscopic observations by the meaning of contact evolution analysis which lead us to introduce two groups of contacts between particles: single and multiple, called simple and complex in that paper. Thus, we observed that complex contacts between clumps transform to simple and that this process depends on the size of concavities, i.e. $\alpha$. We tend to link it with an increase of shear resistance in the case of dense granular samples made of clumps. Focusing on granular assemblies failures, we study shear bands localisation and tried to characterise it by a scalar. It was observed that reflecting shear band were thinner in dense samples made of clumps than ones made of polygons, whatever $\alpha$, highlighting evident geometrical imbrications of clumps that way. In a sense, polygons samples behave more like soil, they slowly create wide shearbands, while clump samples resemble brittle material more.

## Acknowledgments

This work was done as a part of CEGEO research project. The authors would like to express special thanks to F. Radjai, C. Nouguier for fruitful discussions. The authors are indebt to J.-J. Moreau for his guidance on algorithm for contact detection between polygon objects.

## References

[1] J. Lanier, M. Jean, Experiments and numerical simulations with 2D-disks assembly, Powder technology (special issue on Numerical simulations of discrete particle systems) 109 (1–3) (2000) 206–221.

[2] C. Thornton, J. Lanier, Uniaxial compression of granular media: Numerical simulations and physical experiment, in: R. P. Behringer, J. Jenkins (Eds.), Powders and Grains 97, Balkema, Rotterdam, 1997, pp. 223–226.

[3] M. Oda, K. Iwashita (Eds.), Mechanics of granular materials, an introduction, A.A. Balkema, 1999, iSBN 90-5410-461-9.

[4] K. Iwashita, M. Oda, Rotational resistance at contacts in the simulation of shear band development by dem, ASCE Journal of Engineering Mechanics 124 (1998) 285–292.

[5] A. Tordesillas, D. C. Stuart, Incorporating rolling resistance and contact anisotropy in micromechanical models of granular media, Powder Technology 124 (2002) 106–111.

[6] F. Gilabert, J.-N. Roux, A. Castellanos, Computer simulation of model cohesive powders: Influence of assembling procedure and contact laws on low consolidation states, Physical Review E 75 (2007) 011303.

[7] C. Salot, P. Gotteland, P. Villard, Influence of relative density on granular materials behavior: Dem simulations of triaxial tests, Granular Matter - in press.

[8] E. Azema, F. Radjai, R. Peyroux, G. Saussine, Force transmission in a packing of pentagonal particles, Physical Review E (Statistical, Nonlinear, and Soft Matter Physics) 76 (1) (2007) 011301.

[9] P. A. Cundall, O. D. L. Strack, A discrete numerical model for granular assemblies, Géotechnique 29 (1) (1979) 47–65.

[10] D. Rapaport, The Art of Molecular Dynamics Simulation, Cambridge University Press, 1995, iSBN 0-521-82568-7.

[11] J.-N. Roux, G. Combe, On the meaning and microscopic origins of "quasistatic deformation" of granular materials, in: Proceedings of the EM03 ASCE conference, CD-ROM published by ASCE, Seattle, 2003.

[12] M. Allen, D. Tildesley, Computer simulation of liquids, Oxford Science Publications, 1994.

[13] S. Luding, Stress distribution in static two-dimensional granular model media in the absence of friction, Phys. Rev. E 55 (4) (1997) 4720–4729.

[14] M. Hopkins, On the ridging of intact lead ice, Journal of Geophysical Research 99 (1994) 16351,16360.

[15] H.-G. Matuttis, Simulation of the pressure distribution under a two-dimensional heap of polygonal particles, Granular matter 1 (2) (1998) 83–91.

[16] F. Alonso-Marroquin, S. Luding, H. J. Herrmann, I. Vardoulakis, The role of the anisotropy in the elastoplastic response of a polygonal packing, Physical Review E 71 (2005) 051304.

[17] F. Alonso-Marroquin, H. J. Herrmann, Calculation of the incremental stress-strain relation of a polygonal packing, Phys. Rev. E 66 (2) (2002) 021301. doi:10.1103/PhysRevE.66.021301.

[18] J.-J. Moreau, Private communication (2006).

[19] G. Saussine, C. Cholet, P.-E. Gautier, F. Dubois, C. Bohatier, J.-J. Moreau, Modelling ballast behaviour under dynamic loading. part 1: A 2d polygonal discrete element method approach, Computer Methods in Applied Mechanics and Engineering 195 (2006) 2841–2859.

[20] G. Combe, Origines microscopiques du comportement quasi-statique des matériaux granulaires, Ph.D. thesis, Ecole Nationale des Ponts et Chaussées, Champs-sur-Marne, France (2001).

[21] J.-N. Roux, F. Chevoir, Discrete numerical simulation and the mechanical behavior of granular materials, Bulletin des Laboratoires des Ponts et Chaussées 254 (2005) 109–138.

[22] B. Emeriault, B. Cambou, A. Mahboudi, Homogenization for granular materials: non reversible behaviour, Mechanics of cohesive-frictional materials 1 (1996) 199–218.

[23] B. Cambou, P. Dubujet, F. Emeriault, F. Sidoroff, Homogenization for granular materials, European J. of Mechanics A/Solids 14 (1995) 255–276.

[24] J. Bathurst, L. Rothenburg, Micromechanical aspects of isotropic granular assemblies with linear contact interactions, Journal of Applied Mechanics 55 (1988) 17–23.

[25] J. Bathurst, L. Rothenburg, Note on a random isotropic granular material with negative poisson's ratio, International Journal Engineering Science 26 (1988) 373–383.

[26] B. Chareyre, P. Villard, Dynamic spar elements and dem in two dimensions for the modeling of soil-inclusion problems, Journal of Engineering Mechanics 131 (2005) 689–698.

[27] I. Agnolin, J.-N. Roux, Internal states of model isotropic granular packings. i. assembling process, geometry, and contact networks, Physical Review E (Statistical, Nonlinear, and Soft Matter Physics) 76 (6) (2007) 061302.

[28] I. Agnolin, J.-N. Roux, Internal states of model isotropic granular packings. III. Elastic properties., Physical Review E: Statistical, Nonlinear, and Soft Matter Physics 76 (6) (2007) 061304.

[29] F. Calvetti, G. Combe, J. Lanier, Experimental micromechanical analysis of a 2D granular material: relation between structure evolution and loading path, Mechanics of Cohesive-frictional materials 2 (1997) 121–163.

[30] A. Sornette, P. Davy, D. Sornette, Fault growth in brittle-ductile experiments and the mechanics of continental collisions, Journal of geophysical research 98 (1993) 12111–12140.